# **Enhanced Mixing at Low Reynolds Numbers Through Elastic Turbulence**

Chris Goddard and Ortwin Hess

Imperial College London, Department of Physics, London, SW7 2AZ, UK

Reprint requests to C. G.; E-mail: c.goddard@imperial.ac.uk

Z. Naturforsch. 66a, 450-456 (2011); received January 14, 2011

A generic nonlinear Maxwell model for the stress tensor in viscoelastic materials is studied under mixing scenarios in a three-dimensional steady lid-driven cavity flow. Resulting laminar and turbulent flow profiles are investigated to study their mixing efficiencies. Massless tracer particles and passive concentrations are included to show that the irregular spatio-temporal chaos, present in turbulent flow, is useful for potential mixing applications. A Lyapunov measure for filament divergence confirms that the turbulent flow is more efficient at mixing.

Key words: Maxwell-Model Fluid; Turbulence; Mixing.

#### 1. Introduction

Viscoelastic materials display non-Newtonian behaviour under flow, such as shear-thinning/thickening, yield stress, stress relaxation, etc. These can lead to interesting phenomena such as die swell and rod climbing (Weissenberg effect). In low Reynolds number flows elastic turbulence can develop in viscoelastic polymer solutions [1,2] due to elastic instabilities.

High normal stress differences are the cause for secondary flows, which can become irregular, producing turbulent behaviour. A generic description of such a complex rheological behaviour is provided by a generalized nonlinear Maxwell model [3,4]. Depending on the choice of the relevant model parameters, numerical studies of a three-dimensional lid-driven flow, at low Reynolds numbers, demonstrated the occurrence of both laminar and turbulent flow behaviour [5].

In this article we report results on the mixing properties of the lid-driven flow as inferred from this model. The motion of massless tracer particles and the time dependence of passive concentrations reveal the irregular spatio-temporal chaos, present in turbulent flow. A Lyapunov measure for filament divergence confirms that the turbulent flow is more efficient at mixing. On the one hand, the theoretical studies confirm the turbulent nature of the flow. On the other hand, the enhanced mixing achieved in a low Reynolds number turbulent flow is of practical importance for micro-fluidics [6-10]. Modelling of such materials requires a choice for a constitutive relation for the stress, which includes a necessary de-

viation from the simple linear Newtonian description.

#### 2. Maxwell Model

The nonlinear Maxwell model used here was previously studied extensively in spatially homogeneous flow conditions [3, 4, 11]. Recently the model has been applied to a flow geometry which required the analysis of the full three-dimensional hydrodynamic problem [5]. It was observed that a self-generating time-dependent turbulent-like flow regime develops from steady forcing when the nonlinearities in the model are dominant. This response is similar to the experimental work performed by Arratia et al. [12], but in contradistinction to the case of time-periodic flow as studied in [13]. In the following we explore the role of such a turbulent flow for mixing purposes, compared to that of its laminar flow counterpart.

The theoretical description of the hydrodynamic problem is based on the local momentum conservation and a constitutive law for the shear stress tensor. For an incompressible fluid, the relevant equations are  $\rho \, \frac{\mathrm{d} \boldsymbol{v}}{\mathrm{d}t} = -\nabla p + \nabla \cdot \boldsymbol{\sigma} \text{ and } \nabla \cdot \boldsymbol{v} = 0.$ 

The symmetric traceless stress tensor  $\sigma$  is given by the sum of two terms, one involving the second Newtonian viscosity  $\eta_{\infty}$ , the other one the extra stress  $\pi$ , viscoelastic effects can be included,  $\sigma = 2\eta_{\infty}\gamma + \sqrt{2}G_{\rm ref}\pi$ . Here  $G_{\rm ref}$  is a reference shear modulus. Its specific value is not needed for the following analysis.

The dimensionless stress  $\pi$  is assumed to obey the following generalized Maxwell model [3,4]:

$$\frac{\mathrm{d}\boldsymbol{\pi}}{\mathrm{d}t} = 2\boldsymbol{\omega} \times \boldsymbol{\pi} + 2\kappa \boldsymbol{\gamma} \cdot \boldsymbol{\pi} - \tau_0^{-1} (\boldsymbol{\Phi}^{\pi} - \ell_0^2 \nabla^2 \boldsymbol{\pi}) + \sqrt{2} \boldsymbol{\gamma}.$$
(1)

In the above equations,  $\boldsymbol{v}$  is the velocity, p is the pressure,  $\boldsymbol{\gamma}$  is the strain rate tensor,  $\boldsymbol{\omega}$  is the vorticity,  $\kappa$  is akin to a slip parameter in the Johnson–Segalman model [14],  $\tau_0$  is a relaxation time coefficient,  $\ell_0$  is a characteristic length, and  $\boldsymbol{\Phi}^{\boldsymbol{\pi}} \equiv \frac{\partial \boldsymbol{\Phi}}{\partial \boldsymbol{\pi}}$  being the derivative of a potential function with respect to  $\boldsymbol{\pi}$ , where  $\boldsymbol{\Phi}$  is the potential function to be chosen. Here the symbol  $\overline{\cdots}$  represents the symmetric traceless (deviatoric) part of a tensor, e.g.  $\overline{x_{ab}} = \frac{1}{2} (x_{ab} + x_{ba}) - \frac{1}{3} x_{cc} \delta_{ab}$ , where  $\delta_{ab}$  is the unit tensor. The total stress  $\boldsymbol{\sigma}$  is taken as deviatoric, i.e. as symmetric traceless. The substantive (advective) derivative is also used in the above equations,  $\frac{\mathrm{d}}{\mathrm{d}t}(*) \equiv \frac{\partial (*)}{\partial t} + \boldsymbol{u} \cdot \boldsymbol{\nabla}(*)$ .

A generalisation of the Maxwell model with terms nonlinear in the shear stress was invented to treat shear thickening and shear thinning behaviour [3]. A special (simple nontrivial) case for the potential function, which corresponds to an expansion of  $\Phi$  up to terms of fourth order in  $\pi$ , using the second and third-order invariants, thus,

$$\mathbf{\Phi}^{\pi} = A\boldsymbol{\pi} - \sqrt{6}B\overline{\boldsymbol{\pi}\cdot\boldsymbol{\pi}} + C\boldsymbol{\pi}\,\boldsymbol{\pi}:\boldsymbol{\pi}.$$
 (2)

With the stress replaced by the alignment tensor, this expression has the same functional form as that one used to treat the orientational relaxation in molecular fluids and nematic liquid crystals. There, the potential function is essentially the Landau-de Gennes free energy. The equations have been derived within the framework of irreversible thermodynamics [15, 16] and a Fokker-Planck equation [17-19]. Foundations of the equations used here, as well as their dimensionless form and the scaling of variables are discussed in [3-5,11]. Some short remarks are appropriate here. The coefficient A is proportional to  $1 - T^*/T$  whereas B and C are practically independent of the temperature T. The characteristic (pseudo critical) temperature  $T^*$  is below the temperature  $T_c$  where a transition occurs from an ordinary fluid state to a state with a yield stress which is determined by  $\pi_c = 2B/(3C)$ . Dividing  $\pi$  by  $\pi_c$  one obtains a rescaled expression as in (2) with B and C replaced by the numbers 3 and 2, respectively. At the same time A is replaced by  $A^*$  which is defined such that  $A^* = 1$  corresponds to the temperature  $T_c$ . In the rescaled equations it suffices to specify the one coefficient  $A^*$  rather than the values of the original three coefficients A, B, C in order to specify whether the equilibrium state of the system is fluid or one with a yield stress. Furthermore, the time is expressed in units of the relaxation time in fluid state at  $T_c$ . The shear rate is in units of the reciprocal of this time. The link of the present theoretical modelling with a real physical system is made via reference values for the shear stress and the shear rate which are treated as parameters characteristic for a specific substance. Two examples for a comparison with experimental rheological data are given in [11].

The equations, in dimensionless form, are discretized on a regular grid using second-order finite difference approximations for the spatial derivatives. A forth-order Runge–Kutta method is used for the temporal derivatives. The incompressibility condition is implemented using a pressure correction method [20]. A lid-driven cavity flow is chosen with a simple cuboid geometry, and a plate speed such that simulations run with the Reynolds number,  $Re \approx 1$ . The no-slip boundary condition is used for the velocity field, whilst local zero-gradient Neumann conditions are used for  $\pi$ . Simulations are performed on an NEC SX-6 vector supercomputer, more details on the simulation techniques, and preliminary investigations can be found in [5].

### 3. Mixing Dynamics

The time-dependent nature of the flow can be visualized by the paths taken of 'perfect' tracer particles released into the flow [21]. These tracers, which are assumed to have exactly the same flow properties of the containing substance, are allowed to follow the material around freely, but are only influenced by the velocity field in the material. In this way the tracers do not affect the flow and merely provide a way of recording and displaying its history [22].

A similar technique is used in experiments, but there are restrictions on what can be used as it is very unlikely that a perfect tracer can be found. Adding any foreign particles to a material can change its properties, the idea is to find one which has the least effect that is still distinguishable and measurable from the main substance. Often radio-isotopes [23] and high-frequency ultrasonic imaging [24] are used to obtain information about fluid flow.

Many independent particles can be added to give a global picture of the flow, like a long time exposure photograph of illuminated fluid particles. Statistical information about the way a flow can disperse and mix is gathered by analysing particle distributions.

One measure for mixing as a function of time can be obtained by releasing a small cluster of particles in a part of the cavity and then monitoring their evolution. The distribution of points can be measured by the standard deviation of the distances of each point from the mean center of all points. In (3) the standard deviation s(t) is calculated using the position of each particle  $r_i(t)$ , from the center average  $\bar{r}(t)$  of N points,

$$s(t) = \sqrt{\frac{1}{N} \sum_{i=1}^{N} (r_i(t) - \bar{r}(t))^2}.$$
 (3)

Efficient mixing processes are also known to have good stretching and folding of fluid elements, so material filaments are also placed in the fluid to measure stretching [25]. A fluid filament is defined as a one-dimensional length of fluid which is specified by the location of its end points. These end points are treated as massless particles and evolve during flow using the methods outlined above for massless tracer particles.

Filaments of length  $|d\mathbf{X}|$  are initialized, and at time t its new length  $|d\mathbf{x}|$  can be used to calculate a Lyapunov exponent  $\lambda_i$  corresponding to the starting orientation  $\mathbf{M}_i$  around a starting location  $\mathbf{X}$ ,

$$\lambda_i(X, M_i) \equiv \lim_{\substack{t \to \infty \\ |d\mathbf{X}| \to 0}} \left[ \frac{1}{t} \ln \left( \frac{|d\mathbf{x}|}{|d\mathbf{X}|} \right) \right]. \tag{4}$$

It is the sensitivity to initial conditions, present in chaotic systems, that this exponent tries to measure. Normally there are  $N \cdot \mathbf{M}_i$  Lyapunov exponents in an N-dimensional flow, each of which could be a different value. If at least one of the exponents is larger than zero, then the length of the filament increases exponentially with time. The long term average at many points within the cavity will provide a measure for the entire flow. A flow which is better at mixing would be expected to have a larger value for this Lyapunov exponent. A similar experimental technique has been developed recently for studying turbulence in elastic turbulent flow [26].

Much like experimentally adding a dye to a mixing fluid flow, a process of modelling the dispersion of a passive concentration can be performed theoretically. This method is modelled by a scalar concentration which is applied to a volume of fluid evolving under the velocity field, with an added diffusion effect.

The important aspect of diffusion was not covered by any of the previous methods outlined.

A binary fluid is created by assigning concentrations to parts of the fluid. These concentrations are then allowed to mix as the flows are simulated, but do not create any flows themselves, hence being passive. This is a very visual method, which also allows for the identification of areas of unmixed stagnant regions. These are highlighted as regions of the cavity where the mixing action does not reach and whatever initial concentration remains.

Modelling of this concentration is carried out as the simulations are being performed, but could equally be done afterwards if the full velocity field information is retained. The advection of a passive scalar  $\phi$  by an incompressible velocity field v is described by

$$\frac{\partial}{\partial t}\phi + (\mathbf{v} \cdot \nabla)\phi - D_{c}\nabla^{2}\phi = 0, \tag{5}$$

where  $D_c$  is a diffusivity constant.

As before, dimensionless variables are used in the computations. The value  $\phi$  is a concentration quantity which will be transported around the cavity and also allowed to diffuse. By initialising the concentration within the cavity in specific volumes it will be possible to study the mixing as a function of time.

If some initial concentration is left in a cavity with no external forcing, e.g. a zero-velocity field, then diffusion alone will provide the only mixing action. The act of diffusion on its own provides a base measurement for comparisons. Any velocity field which advects the concentrations will speed up the mixing process by moving regions of concentrations to different parts of the cavity. In mixing flows, the process of stretching and folding of fluid elements is the key to efficient mixing.

This method is found to give good results in the high Peclet number regime, when  $D_{\rm c}$  is low enough that the features do not just diffuse away too quickly. For these simulations, a value of  $D_{\rm c}=0.005$ , in reduced units, is used. Whilst this technique is simple to include, it lacks some of the resolution of more advanced adaptive front tracking techniques [27].

To gauge the mixing of the passive concentration, it is necessary to measure statistical properties of the scalar field distributed through the cavity, as a function of time. The ideal end result will be a homogeneous mixed solution throughout the cavity. The value of this homogeneous mixed concentration  $\phi_m$  depends on the amount of concentration added at the start of the pro-

cess. As no concentration is added or lost, an averaging over all grid points at the time of initialisation  $t_s$  will give the value  $\phi_m$ .

At each time step during the mixing, the deviation  $\phi_d$  of the concentration at each grid point  $\phi_p$  from the homogeneous concentration  $\phi_m$  is found from  $\phi_d = |\phi_p - \phi_m|$ .

The average value of  $\phi_d$  throughout the cavity will give an indication of how unmixed the concentration is. The temporal evolution of this quantity will then reveal how efficient each mixing scenario is. The initial distribution for the passive binary solution added to the cavity is chosen to be that of  $\phi_c = 1$  in one half of the cavity split along the *x*-axis, and the rest of the cavity is assigned  $\phi_c = 0$ .

A laminar flow develops when the linear terms in the model (2) dominate, and a single vortex is created inside the cavity. This itself provides a mixing action as the fluid elements are stretched and folded. An example of this single-vortex mixing action is shown in Figure 1 where the lid on top of the box moves towards the right with constant speed. Here the single vortex is very clear and the spiral-like mixing that occurs as a result. The largest Lyapunov exponent calculated for this flow was 0.002. This is very low and practically zero, which would correspond to a stable periodic orbit in any other system of equations.

This single vortex flow presents a vast improvement over the process of just diffusion alone. This is due to the advection of concentration created by the moving fluid driven by the top plate. This creates the much needed stretching and folding action required for good mixing. However, it is apparent that the concentration is trapped by the streamlines and hence mixing can still be improved.

Increasing the top plate velocity has the effect of speeding up the vortex inside of the cavity. This extra velocity results in a speed-up of the mixing process. The stretching part happens at a faster rate in quicker flows, hence the concentration is advected around the cavity faster. The expense of having a faster moving plate is that more energy would be required to drive the mixing apparatus.

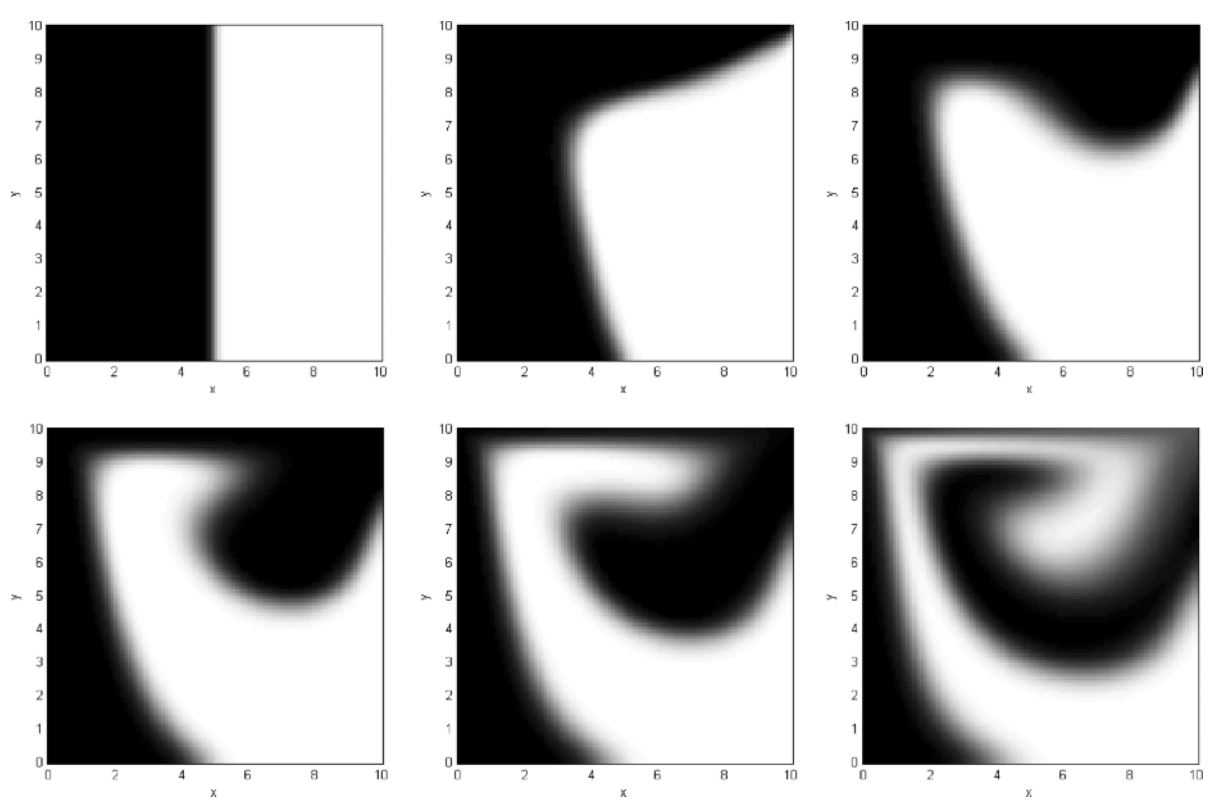


Fig. 1. Laminar flow mixing a passive scalar quantity. A slice is taken through the 3D cavity normal to the driving lid, and parallel to the plate velocity. Snapshots are taken a  $\Delta t = 4.0$  increments.

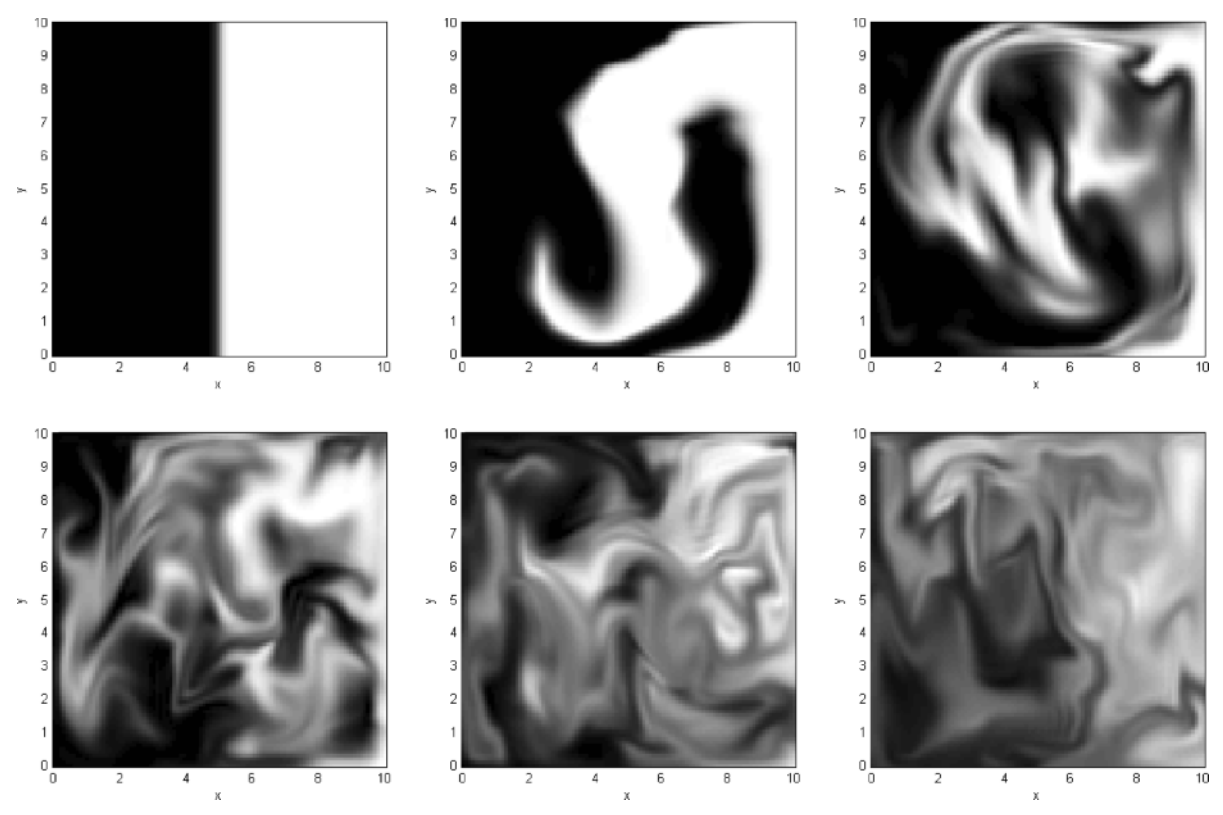


Fig. 2. Turbulent flow mixing of a passive scalar. A slice is taken through the 3D cavity normal to the driving lid, and parallel to the plate velocity. The time increment between snapshots is 4.0.

A turbulent-like flow develops when the nonlinear terms in the model (2) dominate, and an irregular behaviour is observed. Here, a much more efficient mixing occurs compared to that of the laminar regime. High first normal stress differences are observed, which create secondary flows. The nonlinear 'elastic' instability overcomes viscous diffusion to create spatial and temporal chaos.

Figure 2 illustrates an example flow where turbulence has developed, revealed through the mixing of a passive concentration. The spatio-temporal chaotic behaviour of the velocity is revealed through the various time slices, taken at  $\Delta t = 4.0$  increments in time. Different size scales for features can be identified, which appear and disappear as the simulation proceeds. This creates a very effective stretching and folding action, which, coupled with the underlying rate of diffusion results in good mixing. The largest Lyapunov exponent measured for this flow was 0.12.

The path traced by massless particles randomly placed within the cavity can be seen in Figure 3

for laminar and turbulent flows. Here it is observed that the particles are confined to the vortex that is produced in a laminar flow, whilst in the turbulent flow a more irregular path is taken.

The measurement of  $\phi_d(t)$  (from the passive concentration) and s(t) (from tracers) is compared between the different simulations in Figure 4(a) and 4(b), respectively. Here it can be seen that changing the strength of the linear components ( $A^*$ , dimensionless parameter from (2)) has a direct effect on the mixing efficiency. The best mixing occurs at lowest values of  $A^*$ , until flow turns more laminar, when the efficiency is decreased.

As can be inferred from Figure 4(a) at the time t = 40, the laminar flow already enhances the mixing over the pure diffusion by a factor of approximately 2. In the turbulent flow, for  $A^* < 0.3$ , is again enlarged by a factor of about 4.

It is interesting to note that in Figure 4(b) the massless particles are compressed as well as dispersed by the turbulent flow due to its irregular nature. On av-

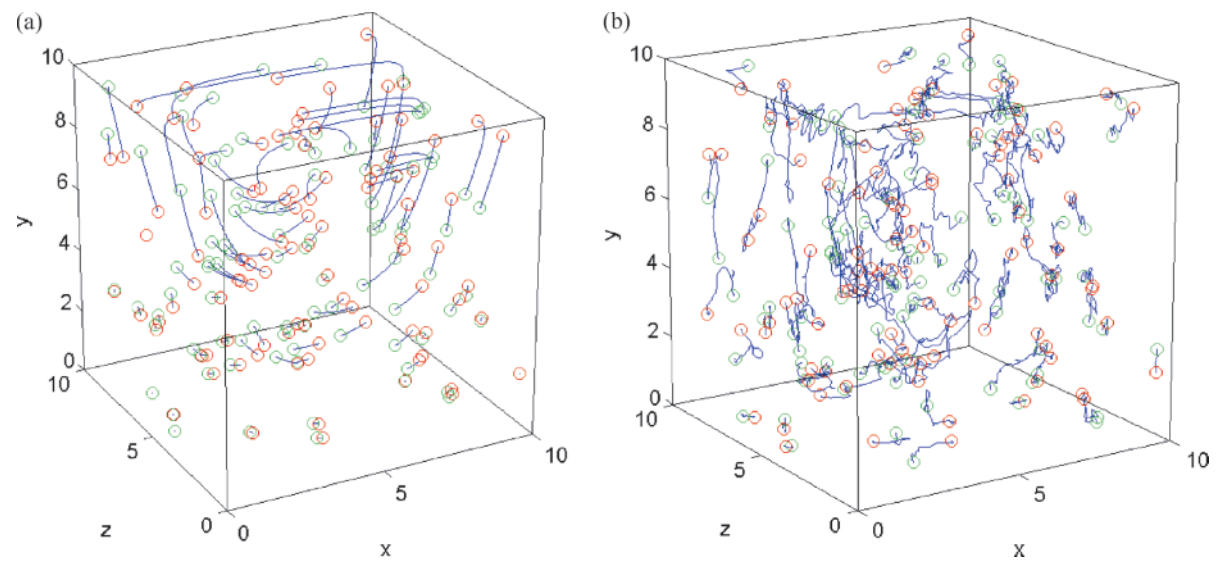


Fig. 3 (colour online). Paths traced by massless particles released at random positions in (a) laminar flow (b) turbulent flow. Red circles mark the starting positions.

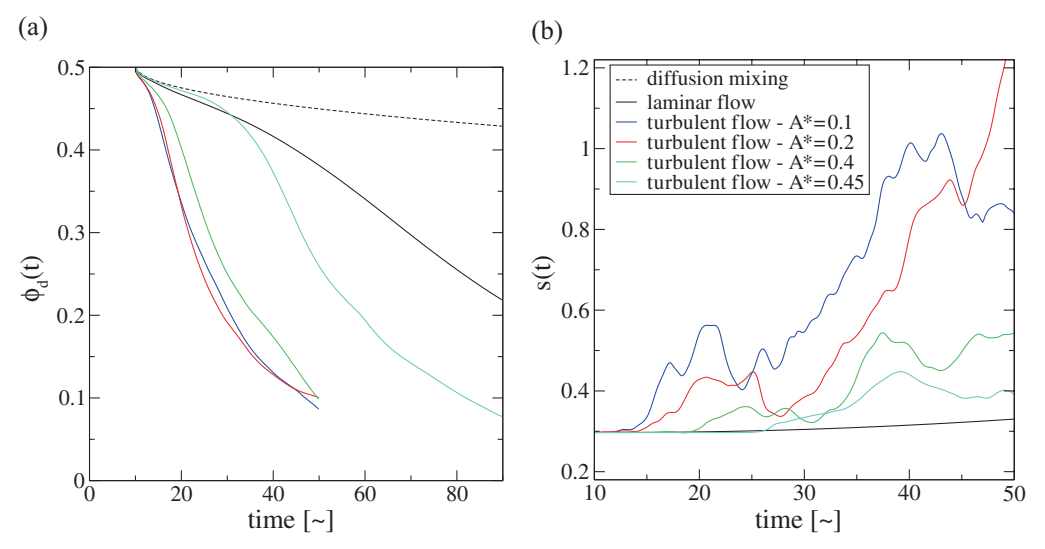


Fig. 4 (colour online). Evolution of (a)  $\phi_d(t)$  and (b) s(t) for the various values of  $A^*$ . Model parameters are the same as those in examples above for comparisons. Tracer concentrations are initialised at t = 10 after a short transient period.

erage the particles tend to move apart, clearly much faster than the pure laminar flow.

## 4. Conclusion

In conclusion, the turbulent flow regime found in a general Maxwell model for viscoelastic materials has

been shown to exhibit far better mixing properties than a laminar counterpart. The spatio-temporal chaotic behaviour of the resulting velocity field creates a stretching and folding action required for good mixing. The measured Lyapunov exponent for turbulent flow was calculated to be 0.12 compared to 0.002 for laminar flow. The temporal evolution of two mix-

ing measures, from massless tracer particles and passive concentrations, revealed the efficiency of each flow. The size of nonlinearities in the equations is identified as a key factor in controlling the mixing rate.

- [1] A. Groisman and V. Steinberg, Nature **405**, 53 (2000).
- [2] R. G. Larson, Nature 405, 27 (2000).
- [3] O. Hess and S. Hess, Physica A **207**, 517 (1994).
- [4] O. Hess, C. Goddard, and S. Hess, Physica A 366, 31 (2006).
- [5] C. Goddard, O. Hess, and S. Hess, Phys. Rev. E 81 036310 (2010).
- [6] H. E. H. Meijer, M. K. Singh, T. G. Kang, J. M. J. den Toonder, and P. D. Anderson, Macromol. Symp 279, 201 (2009).
- [7] A. Dodge, A. Hountondji, M. C. Jullien, and P. Tabeling, Phys. Rev. E 72 056312 (2005).
- [8] A. Dodge, M. C. Jullien, Y. K. Lee, X. Niu, F. Okkels, and P. Tabeling, C.R. Physique 5, 557 (2004).
- [9] E. A. Gibson, D. Schafer, W. Amir, D. W. Marr, J. Squier, and R. Jimenez, In International Conference on Ultrafast Phenomena (UP) (2006).
- [10] T. Burghelea, E. Segre, I. Bar-Joseph, A. Groisman, and V. Steinberg, Phys. Rev. E 69 066305 (2004).
- [11] S. Hess, B. Arlt, S. Heidenreich, P. Ilg, C. Goddard, and O. Hess, Z. Naturforsch. 64a, 81 (2009).
- [12] P. E. Arratia, T. Shinbrot, M. M. Alvarez, and F. J. Muzzio, Phys. Rev. Lett. 94 084501 (2005).
- [13] T. C. Niederkorn and J. M. Ottino, J. Fluid Mech. 256 243 (1993).
- [14] M. W. Johnson and D. Segalman, J. Non-Newtonian Fluid Mechan. 2, 255 (1977).

Acknowledgements

We thank Siegfried Hess for continued interest in this work and for helpful comments. C.G. gratefully acknowledges support from the E.P.S.R.C.

- [15] S. Hess, Z. Naturforsch. **30a**, 728 and 1224 (1975).
- [16] S. Hess, J. Non-Equilib. Thermodyn. 11, 175 (1986).
- [17] S. Hess, Z. Naturforsch. 31a, 1034 (1976).
- [18] M. Doi, Ferroelectrics 30, 247 (1980).
- [19] M. Kröger, Phys. Rep. 390, 453 (2004).
- [20] J. H. Ferziger and M. Perić, Computational Methods for Fluid Dynamics, Springer, Berlin 1997.
- [21] J. S. Brook, J. W. Painter, and D. B. Kothe, Technical report, Los Alamos National Laboratory, Los Alamos, NM 1996.
- [22] P. A. Davidson, Turbulence An Introduction for Scientists and Engineers, Oxford University Press, Oxford 2004.
- [23] E. B. Nauman and B. A. Buffham, Mixing in Continuous Flow Systems, John Wiley & Sons, New York 1983.
- [24] S. Manneville, L. Bécu, P. Grondin, and A. Colin, Colloids Surf. A: Physicochem. Eng. Asp. 270, 195 (2005).
- [25] J. M. Ottino, The Kinematics of Mixing: Stretching, Chaos and Transport, Cambridge University Press, Cambridge 1989.
- [26] T. Burghelea, E. Segre, and V. Steinberg, Europhys. Lett. 68, 529 (2004).
- [27] O. S. Galaktionov, P. D. Anderson, G. W. Peters, and F. N. Van de Vosse, Int. J. Numer. Meth. Fluids 32, 201 (2000).